Publisher: NPG; Journal: Nature: Nature; Article Type: Biology letter
DOI: 10.1038/nature16986

# Sensitivity of global terrestrial ecosystems to climate variability

Alistair W. R. Seddon[1]*, Marc Macias-Fauria[2]*, Peter R. Long[3], David Benz[3] & Kathy J. Willis[1,3,4]

[1]Department of Biology, University of Bergen, Allégaten 41, N-500 Bergen, Norway.

[2]School of Geography and the Environment, South Parks Road, University of Oxford, Oxford OX1 3QY, UK.

[3]Long-term Ecology Laboratory, Biodiversity Institute, Oxford Martin School, Department of Zoology, South Parks Road, University of Oxford, Oxford OX1 3PS, UK.

[4]Royal Botanic Gardens, Kew, Richmond, Surrey TW9 3AB, UK.

*These authors contributed equally to this work.

**The identification of properties that contribute to the persistence and resilience of ecosystems despite climate change constitutes a research priority of global relevance[1]. Here we present a novel, empirical approach to assess the relative sensitivity of ecosystems to climate variability, one property of resilience that builds on theoretical modelling work recognizing that systems closer to critical thresholds respond more sensitively to external perturbations[2]. We develop a new metric, the vegetation sensitivity index (VSI) which identifies areas sensitive to climate variability over the past 14 years. The metric uses time series data of MODIS-derived enhanced vegetation index (EVI)[3] and three climatic variables that drive vegetation productivity[4] (air temperature, water availability and cloud cover). Underlying the analysis is an autoregressive modelling approach used to identify climate drivers of vegetation productivity on monthly timescales, in addition to regions with memory effects and reduced response rates to external forcing[5]. We find ecologically sensitive regions with amplified responses to climate variability in the arctic tundra, parts of the boreal forest belt, the tropical rainforest, alpine regions worldwide, steppe and prairie regions of central Asia and North and South America, the Caatinga deciduous forest in eastern South America, and eastern areas of Australia. Our study provides a quantitative methodology for assessing the relative response rate of ecosystems—be they natural or with a strong anthropogenic signature—to environmental variability, which is the first step toward addressing why some regions appear to be more sensitive than others and what impact this has upon the resilience of ecosystem service provision and human well-being.**

The rate and scale of projected climate changes in the 21st century are likely to have profound impacts on the functioning of Earth's ecosystems[6]. Much current understanding of how biodiversity will respond to climate change is based on responses to changes in mean

Publisher: NPG; Journal: Nature: Nature; Article Type: Biology letter
DOI: 10.1038/nature16986

climate state[7]. However, climate variability, and the related increases in extreme events in a warmer world[8], has a strong influence on both the structuring and functioning of ecosystems[9–11]. Given the importance of identifying ecologically sensitive areas for ecosystem service provision and poverty alleviation[1], a key knowledge gap exists in how to identify and then prioritize those regions that are most sensitive to climatic variability.

Ecosystem response to variability in external forcing is a key component of resilience. Theory indicates that systems with lower resilience (that is, those with a high probability of crossing a threshold to an alternative state[12]) experience amplified responses to disturbance and are more sensitive to environmental perturbations[2]. In addition, slower responses (identified through increased autocorrelation) may be evidence of reduced recovery rates in systems approaching critical transitions[13]. Therefore, identification of areas with high ecological sensitivity or reduced recovery rates is an important step in recognizing regions of pending ecological change. In the past decade there has been an increase in the availability of satellite data measuring climate and other ecologically relevant variables[14]. These data offer opportunities to characterize ecosystem sensitivity, potentially a key component of resilience, at a global scale and at high spatial resolution.

We present a novel method to identify ecosystem sensitivity to short-term climate variability and regions of amplified vegetation response (see Methods and Extended Data Fig. 1). We develop a new metric, the vegetation sensitivity index (VSI), which independently compares the relative variance of vegetation productivity (EVI)[3] with that of three ecologically important MODIS-derived climate variables[4] (air temperature[15], water availability[16] and cloud-cover)[17] for each 5 km grid square for the months in which EVI and climate are found to be related. Climate–vegetation-productivity relationships are determined using an AR1 multiple linear regression approach, which uses the three climate variables and one-month-lagged vegetation anomalies (see Methods) to identify areas with strong vegetation coupling to climate anomalies (Extended Data Fig. 2). The coefficient from the one-month-lagged vegetation-productivity anomalies can be used to identify regions with memory effects, highlighting the importance of past ecosystem conditions in these regions[5] (Extended Data Fig. 3). Our global VSI then results from aggregating the EVI sensitivities to each climate variable, weighted by the coefficients from the linear regression modelling (see Methods and Extended Data Fig. 2).

Our analysis provides three key insights into the patterns and drivers of ecological sensitivity and response to climate forcing at a global scale. First, we identify areas exhibiting

Publisher: NPG; Journal: Nature: Nature; Article Type: Biology letter
DOI: 10.1038/nature16986

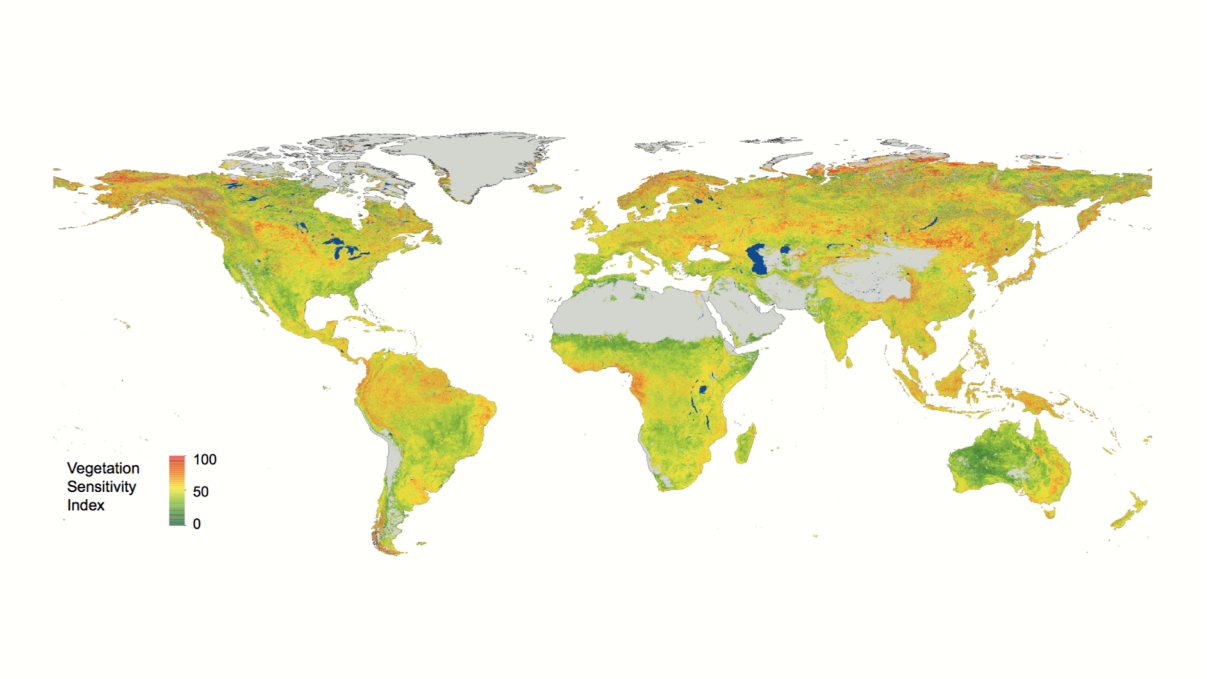


**Figure 1 Vegetation sensitivity index.** Sensitivity of vegetation productivity (defined as EVI) to climate variability (based on temperature, water availability and cloudiness). The index ranges from 0 (low sensitivity, green) to 100 (high sensitivity, red). Areas with dominant barren land (mean EVI < 0.1 for all months) and permanent ice are shown grey. Wetland areas, as identified by the Global Lakes and Wetlands Database[30], are mapped in blue. Pixel resolution, 5 km; period, 2000–2013. Continental outlines were modified from a shapefile using ArcGIS 10.2 software (http://www.arcgis.com/home/item.html?id=a3cb207855b348a297ab85261743351d). ArcGIS and ArcMap are the intellectual property of Esri and are used herein under license.

amplified responses to climate variability (Fig. 1). The Arctic tundra, parts of the boreal forest belt, the wet tropical forests of South America, western Africa, and southeast Asia/ New Guinea, alpine regions worldwide, steppe and prairie regions of central Asia and North and South America, the Caatinga deciduous forest in eastern South America, and eastern areas of Australia displayed high VSI values, indicating a high sensitivity to climate variability over the past 14 years. The relative contribution of each climate variable to vegetation sensitivity can also be assessed (Fig. 2). Whereas the Caatinga biome in Brazil and the prairie and grassland regions of North America and Asia are most sensitive to variations in water availability, alpine regions (for example, the Andes) demonstrate strong sensitivity to temperature, and high-latitude tundra areas exhibit strong responses to both temperature and cloud cover variability. The high sensitivity to monthly changes in cloudiness and temperature in tropical forests is also noteworthy.

Publisher: NPG; Journal: Nature: Nature; Article Type: Biology letter
DOI: 10.1038/nature16986

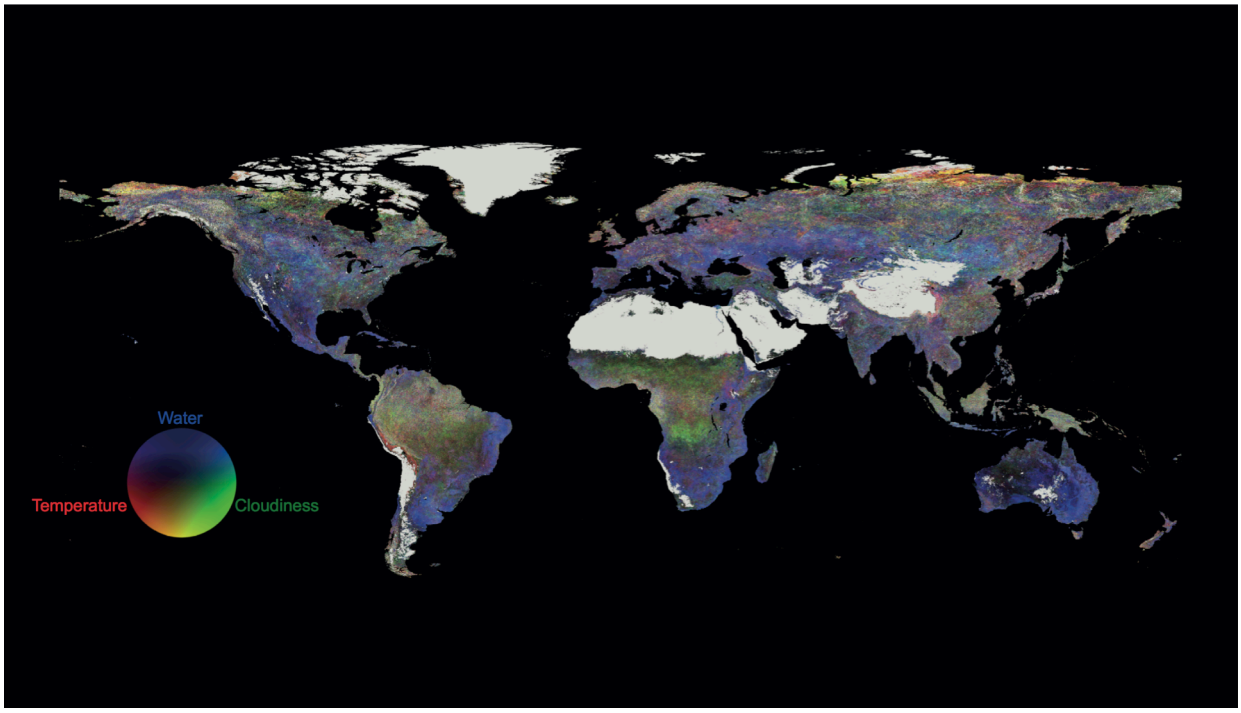


**Figure 2 RGB composite of vegetation sensitivity index.** Global contribution of three climate variables to the vegetation sensitivity index (temperature, red; water availability, blue; and cloudiness, green). Pixel resolution, 5 km; period, 2000–2013. Areas with dominant barren land (mean EVI < 0.1 for all months) and permanent ice are shown grey.

Second, we present an empirical approach to quantify climate drivers of vegetation productivity (that is, the weights related to the three climate variables derived from the AR1 linear regression, Extended Data Fig. 2, hereafter climate weights, see Methods). This represents a major advancement from previous studies which have used hypothesized ecological tolerance limits to determine the relative importance of different variables driving productivity[4]. The overall picture from our empirical analysis is remarkably similar to this previous conceptual modelling exercise[4]: prairies in mid-northern hemisphere latitudes are water limited, the high-latitudes are driven by a combination of temperature and cloudiness, and tropical forests show strong responses to cloudiness. Nevertheless, a number of key differences with this previous study are also observed. For example, central and western continental Europe exhibit stronger water limitation compared to the modelling study (as compared to temperature and radiation – a variable linked to cloudiness), while water limitation was also found to be an important driver in central Africa (as compared to radiation[4]). A key question remains as to whether these differences result from modelling

assumptions, or whether changing climate in the last 14 years has resulted in diverging vegetation responses in these regions.

Third are the areas with high variance explained by the $t-1$ variable in the AR1 model, indicating systems where memory effects play a more important role than contemporary climate conditions in determining vegetation productivity[5] (Extended Data Fig. 3). Overall, areas with low VSI values showed the largest memory effects (that is, high $t-1$ coefficients in our AR1 model), including the drylands of the Sahel, Australian outback, southwest USA, and the Middle East. Assessment of time series in these regions indicates that the apparent lack of response to the other climate variables occurs in two main ways: constant and largely stable low productivity conditions despite large climate variability (that is, high ecological resilience to climatic (mostly precipitation) variability, for example, Australian outback), or strong cyclical variability with periods of very low and stable EVI (for example, Sahel; Extended Data Fig. 4). This contrasts to water-limited areas with higher mean EVI (for example, prairies), where strong seasonal variability is observed (Extended Data Fig. 4). Since the importance of 12-month-lagged responses in dryland regions has been previously identified[18], we also tested whether model performance improved using lags of up to one year (not shown). However, we found that a one-month lag provided the best explanatory power for vegetation responses to variability on these timescales. We also found that the strength of the $t-1$ coefficient increases with decreasing levels of total annual precipitation, while there was a small positive effect on the magnitude of the climate weight related to water availability as total annual precipitation increased (Extended Data Fig. 5). These results probably indicate the importance of lagged responses to precipitation input as a result of processes related to soil-water recharge in arid regions[19].

These empirically determined patterns agree with the results of multiple studies with regards to understanding current vegetation responses to climate change. Arctic and boreal regions have experienced the most rapid rates of warming in the past 30 years[20] and there is ample evidence on enhanced shrub growth in the tundra as a response to warming temperatures[21,22]. We also observe similar patterns in alpine and mountainous ecosystems, adding to the increasing evidence that such areas are responding rapidly to climate change[6]. Our analysis also reveals high sensitivity to a combination of cloudiness and temperature variability in the tropical rainforest regions, particularly in the Amazon and southeast Asia (Fig. 2). Although the extent to which tropical ecosystems are currently operating at their thermal limits remains uncertain, a number of studies have found decreases in tropical forest

growth rates and productivity in response to warming[23], potentially the result of reductions of leaf gas exchange under warmer temperatures[24]. Such findings may have implications for the future of tropical forests since they are projected to experience temperature ranges beyond any current analogues[25]. The high sensitivity to monthly changes in cloud cover and temperature in tropical forests observed in this study may be operating at different timescales to potential precipitation thresholds that have been identified in tropical forests[26]. By contrast, the enhanced sensitivity to water availability in the Caatinga region of northeast Brazil agrees with studies which indicate strong coupling of vegetation cover and phenology to ENSO-related precipitation change[27]. One potential explanation is that the high phenotypic plasticity of leaf senescence and green-up results in large amplitudes in the EVI response to drought variability. Understanding the traits that result in sensitivity differences worldwide is a key research priority.

We identified regions with high rates of response to climate variability globally and at high spatial and temporal resolutions. These properties have been linked to systems approaching ecological tipping points[2]. However, whereas the existence of critical ecological thresholds has been suggested for a number of regions with high VSI values, such as the Arctic tundra, the boreal forest, and the wet tropical forests[26], some high VSI areas (for example, the steppe and prairies or the Caatinga) have not been reported to exhibit threshold-type responses at global scales[26]. As presented, VSI is an empirically calculated state variable of ecological sensitivity for the last 14 years. As longer records of remotely sensed global vegetation and climate become available in the future, VSI offers the opportunity to identify areas showing increasing or decreasing trends in ecological sensitivity, with possible implications for identifying critical thresholds. Finally, since there is little overlap between areas demonstrating strong memory effects and those with high VSI, a question remains as to what fundamental properties underlie the difference behind fast-responding and slow-responding systems.

Identification of large-scale metrics to quantify ecological responses to climate change remains a vital strategy for global ecosystem assessment. This work builds on previous studies identifying properties that represent components of ecological resilience using satellite data[5,28,29]. Our novel approach provides empirical baseline measurements on a key component of ecosystem resilience, that is, the relative response of vegetation in comparison to environmental perturbations over time, as well as the climatic drivers of change across landscapes globally. The next challenge is to understand the underlying causes and ecological processes that lead to these patterns. It is also critical to determine whether these patterns

represent long-lasting characteristics of the ecosystems/habitats, apparent over decades to millennia, or else more transient responses able to change spatially over short time scales, and to develop tools and technologies for modelling and predicting future trends.

Received 19 June 2015; accepted 12 January 2016.

Published online XX 2016.

<eref>1. Convention on Biological Diversity, Aichi biodiversity targets. <http://www.cbd.int/sp/targets/default.shtml></eref>

<jrn>2. Scheffer, M. *et al.* Early-warning signals for critical transitions. *Nature* **461,** 53–59 (2009). Medline CrossRef</jrn>

<eref>3. Solano, R., Didan, K., Jacobson, A. & Huete, A. MODIS vegetation index C5 user's guide (MOD13 Series). 1–42 (2010) <http://vip.arizona.edu/documents/MODIS/MODIS_VI_UsersGuide_01_2012.pdf></eref>

<jrn>4. Nemani, R. R. *et al.* Climate-driven increases in global terrestrial net primary production from 1982 to 1999. *Science* **300,** 1560–1563 (2003). Medline CrossRef</jrn>

<jrn>5. De Keersmaecker, W. *et al.* A model quantifying global vegetation resistance and resilience to short-term climate anomalies and their relationship with vegetation cover. *Glob. Ecol. Biogeogr.* **24,** 539–548 (2015). CrossRef</jrn>

<jrn>6. Garcia, R. A., Cabeza, M., Rahbek, C. & Araujo, M. B. Multiple dimensions of climate change and their implications for biodiversity. *Science* **344,** 1247579 (2014). Medline CrossRef</jrn>

<jrn>7. Thomas, C. D. *et al.* Extinction risk from climate change. *Nature* **427,** 145–148 (2004). Medline CrossRef</jrn>

<jrn>8. Kharin, V. V., Zwiers, F. W., Zhang, X. & Hegerl, G. C. Changes in temperature and precipitation extremes in the IPCC ensemble of global coupled model simulations. *J. Clim.* **20,** 1419–1444 (2007). CrossRef</jrn>

<jrn>9. Holmgren, M., Hirota, M., Van Nes, E. H. & Scheffer, M. Effects of interannual climate variability on tropical tree cover. *Nature Clim. Change* **3,** 755–758 (2013). CrossRef</jrn>

<jrn>10. Pederson, N. *et al.* The legacy of episodic climatic events in shaping temperate, broadleaf forests. *Ecol. Monogr.* **84,** 599–620 (2014). CrossRef</jrn>

<jrn>11. Doughty, C. E. *et al.* Drought impact on forest carbon dynamics and fluxes in Amazonia. *Nature* **519,** 78–82 (2015). Medline CrossRef</jrn>

<jrn>12. Holling, C. S. Resilience and stability of ecological systems. *Annu. Rev. Ecol. Evol. Syst.* **4,** 1–23 (1973). CrossRef</jrn>

<jrn>13. Dakos, V. *et al.* Slowing down as an early warning signal for abrupt climate change. *Proc. Natl Acad. Sci. USA* **105,** 14308–14312 (2008). Medline CrossRef</jrn>

<jrn>14. Kerr, J. T. & Ostrovsky, M. From space to species: ecological applications for remote sensing. *Trends Ecol. Evol.* **18,** 299–305 (2003). CrossRef</jrn>

<eref>15. Seeman, S. W., Borbas, E. E., Li, J., Menzel, W. P. & Gumley, L. E. MODIS atmospheric profile retrieval algorithm theoretical basis document, version 6. (2006) <http://modis-atmos.gsfc.nasa.gov/_docs/MOD07MYD07ATBDC005.pdf></eref>

<jrn>16. Mu, Q., Zhao, M. & Running, S. W. Improvements to a MODIS global terrestrial evapotranspiration algorithm. *Remote Sens. Environ.* **115,** 1781–1800 (2011). CrossRef</jrn>

<eref>17. Ackerman, S. *et al.* Discriminating clear-sky from cloud with MODIS: algorithm theoretical basis document (MOD35), version 6.1. (2010) <http://modis-atmos.gsfc.nasa.gov/_docs/MOD35_ATBD_Collection6.pdf ></eref>

<jrn>18. Sala, O. E., Gherardi, L. A., Reichmann, L., Jobbagy, E. & Peters, D. Legacies of precipitation fluctuations on primary production: theory and data synthesis. *Phil. Trans. R. Soc. Lond. B* **367,** 3135–3144 (2012). Medline CrossRef</jrn>

<jrn>19. Richard, Y. & Poccard, I. A statistical study of NDVI sensitivity to seasonal and interannual rainfall variations in southern Africa. *Int. J. Remote Sens.* **19,** 2907–2920 (1998). CrossRef</jrn>

<bok>20. *Climate Change 2013: The Physical Science Basis*. (Cambridge University Press, 2013).</bok>

<jrn>21. Macias-Fauria, M., Forbes, B. C., Zetterberg, P. & Kumpula, T. Eurasian Arctic greening reveals teleconnections and the potential for structurally novel ecosystems. *Nature Clim. Change* **2,** 613–618 (2012). CrossRef</jrn>

<jrn>22. Myers-Smith, I. H. *et al.* Shrub expansion in tundra ecosystems: dynamics, impacts and research priorities. *Environ. Res. Lett.* **6,** 045509 (2011). CrossRef</jrn>

<jrn>23. Clark, D. A., Piper, S. C., Keeling, C. D. & Clark, D. B. Tropical rain forest tree growth and atmospheric carbon dynamics linked to interannual temperature variation during 1984 –2000. *Proc. Natl Acad. Sci. USA* **100,** 5852–5857 (2003). Medline CrossRef</jrn>

<jrn>24. Doughty, C. E. & Goulden, M. L. Are tropical forests near a high temperature threshold? *J. Geophys. Res.* **113,** G00B07 (2008). CrossRef</jrn>

<jrn>25. Williams, J. W., Jackson, S. T. & Kutzbach, J. E. Projected distributions of novel and disappearing climates by 2100 AD. *Proc. Natl Acad. Sci. USA* **104,** 5738–5742 (2007). Medline CrossRef</jrn>

<jrn>26. Lenton, T. M. *et al.* Tipping elements in the Earth's climate system. *Proc. Natl Acad. Sci. USA* **105,** 1786–1793 (2008). Medline CrossRef</jrn>

<jrn>27. Barbosa, H. A., Huete, A. R. & Baethgen, W. E. A 20-year study of NDVI variability over the northeast region of Brazil. *J. Arid Environ.* **67,** 288–307 (2006). CrossRef</jrn>

<jrn>28. Harris, A., Carr, A. S. & Dash, J. Remote sensing of vegetation cover dynamics and resilience across southern Africa. *Int. J. Appl. Earth Obs. Geoinf.* **28,** 131–139 (2014). CrossRef</jrn>

<jrn>29. Hirota, M., Holmgren, M., Van Nes, E. H. & Scheffer, M. Global resilience of tropical forest and savanna to critical transitions. *Science* **334,** 232–235 (2011). Medline CrossRef</jrn>

<jrn>30. Lehner, B. & Döll, P. Development and validation of a global database of lakes, reservoirs and wetlands. *J. Hydrol. (Amst.)* **296,** 1–22 (2004). CrossRef</jrn>

**Acknowledgements** This work was funded by Statoil ASA, Norway, Contract number 4501995279 (K.J.W., A.W.R.S., D.B.), and by the European Commission LIFE12 ENV/UK/000473 (K.J.W., D.B. and P.R.L.). P.R.L. was also supported by an Oxford Martin School Fellowship. M.M.-F. was supported by a Natural Environment Research Council Independent Research Fellowship (NE/L011859/1) and A.W.R.S. was supported by a Research Council of Norway Postdoctoral Fellowship within a FRIMEDBIO project grant (FRIMEDBIO-214359) during analysis and write-up of this work.

Publisher: NPG; Journal: Nature: Nature; Article Type: Biology letter
DOI: 10.1038/nature16986

**Author Contributions** All authors designed the study. D.B. and P.R.L. prepared and downloaded the remote-sensing data and A.W.R.S. and M.M.-F. carried out the data analysis. A.W.R.S., M.M.-F. and K.J.W. co-wrote the paper, with contributions from D.B. and P.R.L.

**Author Information** Remote sensing data are uploaded in the ORA repository (https://oradeposit.bodleian.ox.ac.uk/, DOI:10.5287/bodleian:VY2PeyGX4) .Reprints and permissions information is available at www.nature.com/reprints. The authors declare no competing financial interests. Readers are welcome to comment on the online version of the paper. Correspondence and requests for materials should be addressed to A.W.R.S. (alistair.seddon@bio.uib.no).

**Code availability** All code used to conduct this analysis is available online from the ORA repository https://oradeposit.bodleian.ox.ac.uk/, DOI:10.5287/bodleian:VY2PeyGX4.

## METHODS

### Satellite data

We derived monthly time series of four key ecosystem and climate variables from the MODIS sensor for the period February 2000 to December 2013. To obtain estimates of changes in ecosystem productivity, we used the MOD13C2 version 5 product which comprises monthly, global enhanced vegetation index (EVI) at 0.05° resolution[3]. EVI is a normalized ratio of reflectance bands with a practical range of 0 to 1. Higher values result from absorption in the visible red band of the electromagnetic spectrum. The index correlates strongly with chlorophyll content and photosynthetic activity[31]. In some cases where no clear-sky observations are available, the MOD13C2 version 5 product replaces no-data values with climatological monthly means, so we removed these values where appropriate.

We used the MOD07_L2 Atmospheric Profile product as a measure of air temperature at the same spatial resolution[15]. Five-minute swaths of retrieved temperature profile were projected to geographic coordinates. Pixels from the highest available pressure level, corresponding to the temperature nearest the Earth's surface, were selected in each swath. Swaths were then mean-mosaicked into global daily images, and daily images were mean-composited to monthly images to provide global time series of temperature at 0.05° resolution.

No direct estimates of incoming radiation are available from the MODIS sensor. Therefore, we developed an insolation proxy based on the MOD35_L2 Cloud Mask product[17]. This product provides daily records on the presence of cloudy versus cloudless skies, and we used this to make an index of the proportion of cloudy to clear-sky days in a given pixel. After conversion to geographic coordinates, five-minute swaths at 1 km resolution were re-classed as

clear sky or cloudy, and these daily swaths were mean-mosaicked to global coverage, mean-composited from daily to monthly, and mean aggregated from 1 km to 0.05°. An example output from June 2005 is provided in Extended Data Fig. 6. Note that we observed a sampling bias in the MODIS insolation data at approximately 60° N in northern Eurasia, but this bias tends to occur in low insolation months between November and January and so does not influence the overall results.

The ratio of actual evapotranspiration to potential evapotranspiration (AET/PET) was used as an indicator of water availability. A value close to 1 indicates sufficient water supply to the plant, since all incoming photosynthetically active solar radiation is being used for photosynthesis. Monthly, 0.05° AET/PET was calculated from the MOD16 Global Evapotranspiration product, which estimates AET and PET through the Penman–Monteith equation[16,32].

**Climatic drivers of vegetation productivity**

To estimate the relative importance of the three climate variables driving monthly changes in productivity, all time series were transformed to *z*-score anomalies using monthly climatology means and standard deviations. Any month with a mean EVI below 0.1 was removed from the analysis to reduce the potential impact of noisy data at low EVI values, which are attributed to areas with extremely sparse or inexistent vegetation cover. We also removed months with a mean monthly temperature of less than 0 °C. We then used a multiple regression approach to test for linear relationships with climate. We included the one-month-lagged EVI monthly anomalies as a fourth variable in this regression to investigate the potential influence of memory effects driving vegetation productivity (Extended Data Figs 1–3). To remove any impact of co-linearity between the three climate predictor variables[33], we used a principal components regression (PCR) to identify the relative importance of each variable driving monthly variations of EVI in each pixel. For those principal components found to have significant relationships with climate ($P < 0.1$, Extended Data Fig. 7), we multiplied the loading scores of each variable by the PCR coefficients and summed these scores. This enabled us to estimate the relative importance of each variable in driving monthly changes in productivity. Finally, we found the mean, absolute value of the variable-transformed PCR coefficients providing an empirical approach to map the relative importance of climate on productivity globally (hereafter, climate weights). The climate weights from each variable were rescaled between 0 and 1 (using the minimum and maximum value of any of the climate coefficient values) to be used for our calculations of ecological sensitivity.

Publisher: NPG; Journal: Nature: Nature; Article Type: Biology letter
DOI: 10.1038/nature16986

**Vegetation sensitivity index**

To estimate ecosystem sensitivity globally, we created seasonally de-trended time series (mean monthly values subtracted) of each variable for each pixel and for periods found to have an relationship with climate and the $t-1$ variable in our monthly principal components regressions. We estimated the variance of both the climatic variables and EVI on these time series. Because we found a relationship between the variance and the mean of the different months, the residuals of a quadratic linear model fitted to the mean–variance relationship of both EVI and the climate variables for each pixel were used (Extended Data Fig. 8). We standardized these residuals to between 0 and 100 for each variable. Our sensitivity metrics are the $\log_{10}$-transformed ratios of EVI variability and each of the climate variables. Each ratio was then weighted according to the importance of the climate variable to EVI variability by multiplying it by the value of the regression coefficient (climate weights). Finally, we summed the sensitivity scores for each of our variables to identify areas of enhanced variability for the period of study (Fig. 1). All data analyses were carried out using the R project for statistical computing[34], using the raster[35], nlme[36], gstat[37], rgdal[38] and gtools[39] packages. Image processing was also carried out using Python 2.7, ArcGIS 10.2, Idrisi Selva, and the HDF-EOS to GeoTIFF Conversion Tool.

**Uncertainty layers**

We provide a series of maps assessing uncertainty both in the EVI measurements and in the algorithm used. In order to assess whether noise resulting from cloudy observations may be a concern to interpretations in tropical forest locations, we computed a map of the average standard error of the mean EVI score calculated for each month, which is a useful metric for identifying areas of high uncertainty in the vegetation time series (Extended Data Fig. 9). This is based on the standard deviation and number of valid EVI observations, both of which can be obtained within the metadata of the MODIS product. The highest standard errors are observed in areas with periodic presence of water on the surface (for example, Amazon river, wetlands), which is interpreted as large differences within the EVI observations and within a given month as a function of rapid, intra-month changes in the presence of surface water. Moderately high standard errors are observed in areas with more cloud cover, including parts of the wet tropical forests, the northwest coasts of Europe and North America, and some mountain ranges such as the Alps, the Pyrenees, or the Canadian Rocky Mountains. The absolute values of standard errors are not high and do not compromise the interpretation of results and their robustness: monthly EVI means for all pixels were computed from at least 25 observations on average

(except for small areas in western Ecuador and Colombia, Borneo and Papua, which were based on at least 15 observations per month on average), and the monthly mean EVI standard deviation for over 90% of Earth was smaller than 0.08 (for EVI values ranging from 0 to 1).

In order to assess uncertainty in our results further, we also computed confidence interval maps for every variable implemented in the regression between EVI and climate (Extended Data Fig. 10a–d). These maps were calculated by finding the upper and lower confidence intervals in the PCA regression, before transforming them back to the scale of the original climate variables using the PCA weights. We then scaled these confidence intervals by the original variables to determine uncertainty in the regression coefficients as compared to the size of the coefficients (resulting in normalized confidence interval amplitudes (NCIA)). Here, a value of 2 corresponds to a total uncertainty twice as big as the coefficient value. This analysis indicates that for all variables, NCIA is lowest where the coefficients are highest, and that the absolute NCIA values are well within acceptable levels.

**Code availability**

All R and MATLAB code is available for download alongside the raw data files in the ORA repository. http://www.bodleian.ox.ac.uk/ora, DOI:10.5287/bodleian:VY2PeyGX4.

<jrn>31. Huete, A. *et al.* Overview of the radiometric and biophysical performance of the MODIS vegetation indices. *Remote Sens. Environ.* **83,** 195–213 (2002). CrossRef</jrn>

<jrn>32. Cleugh, H. A., Leuning, R., Mu, Q. & Running, S. W. Regional evaporation estimates from flux tower and MODIS satellite data. *Remote Sens. Environ.* **106,** 285–304 (2007). CrossRef</jrn>

<bok>33. Zuur, A. F., Ieno, E. N. & Smith, G. M. *Analyzing Ecological Data*. (Springer, 2007).</bok>

<eref>34. R Core Team. R: A language and environment for statistical computing. (2015) <http://www.R-project.org/></eref>

<eref>35. Hijmans, R. J. raster: geographic data analysis and modeling. R package version 2.4-20. (2015) <http://CRAN.R-project.org/package=raster></eref>

<eref>36. Pinheiro, J., Bates, D., Debroy, S., Sarkar, D. & Team, A. T. R. D. C. nlme: linear and nonlinear mixed effects models. R package version 3.1-122. (2013) <http://CRAN.R-project.org/package=nlme>.</eref>

<jrn>37. Pebesma, E. J. Multivariable geostatistics in S: the gstat package. *Comput. Geosci.* **30,** 683–691 (2004). CrossRef</jrn>

<eref>38. Bivand, R., Keitt, T. & Rowlingson, B. rgdal: bindings for the geospatial data abstraction library. R package version 0.9-3. (2015) <http://CRAN.R-project.org/package=rgdal></eref>

<eref>39. Warnes, G. R., Bolker, B. & Lumley, T. gtools: various R programming tools. R package version 3.5.0. (2015) <http://CRAN.R-project.org/package=gtools></eref>

<jrn>40. Hijmans, R. J., Cameron, S. E., Parra, J. L., Jones, P. G. & Jarvis, A. Very high resolution interpolated climate surfaces for global land areas. *Int. J. Climatol.* **25,** 1965–1978 (2005). CrossRef</jrn>

<eref>41. Pope, N. corHaversine function. (2013) <http://stackoverflow.com/questions/18857443/specifying-a-correlation-structure-for-a-linear-mixed-model-using-the-ramps-pack></eref>

Publisher: NPG; Journal: Nature: Nature; Article Type: Biology letter
DOI: 10.1038/nature16986

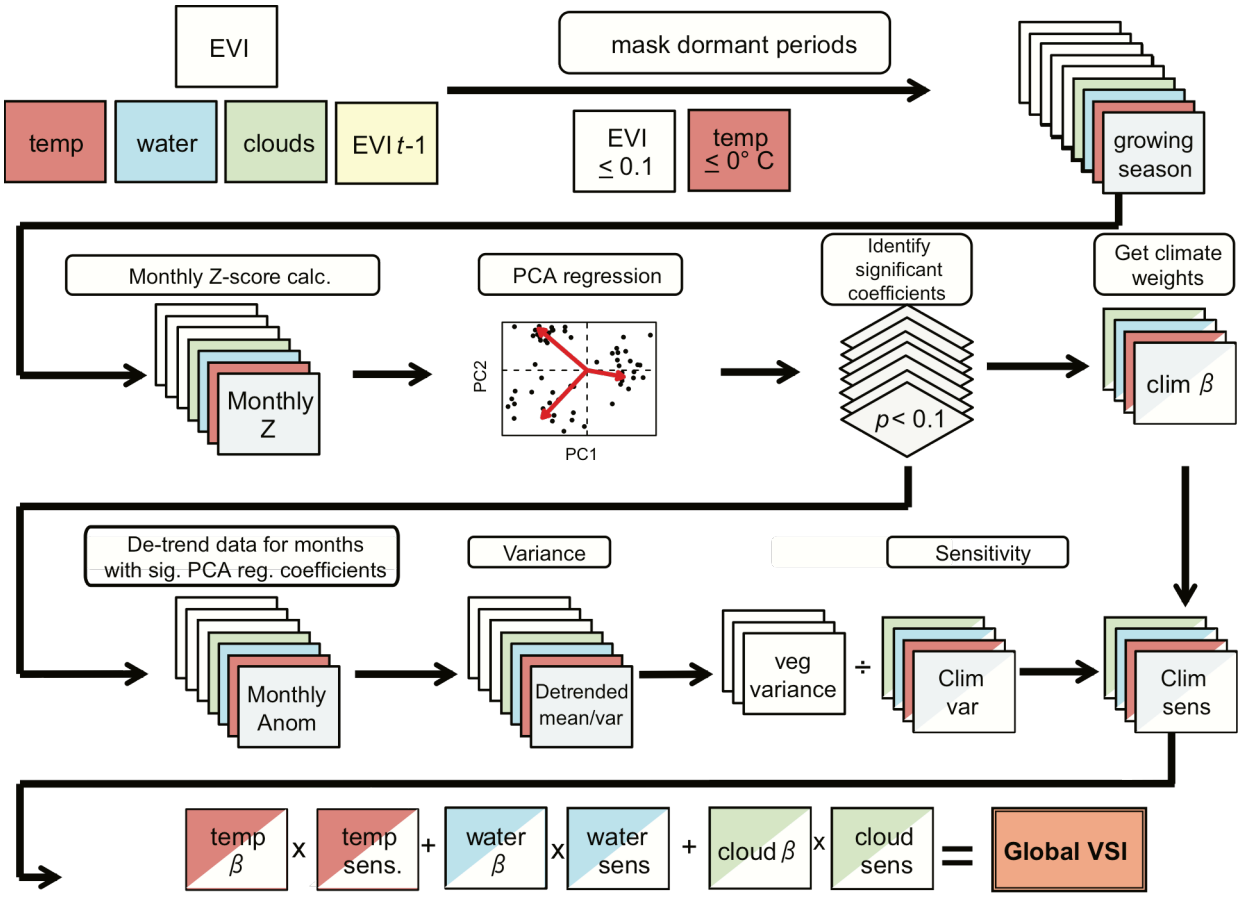


**Extended Data Figure 1 Study Design.** Flow chart of the algorithm used to estimate the vegetation sensitivity index.

Publisher: NPG; Journal: Nature: Nature; Article Type: Biology letter
DOI: 10.1038/nature16986

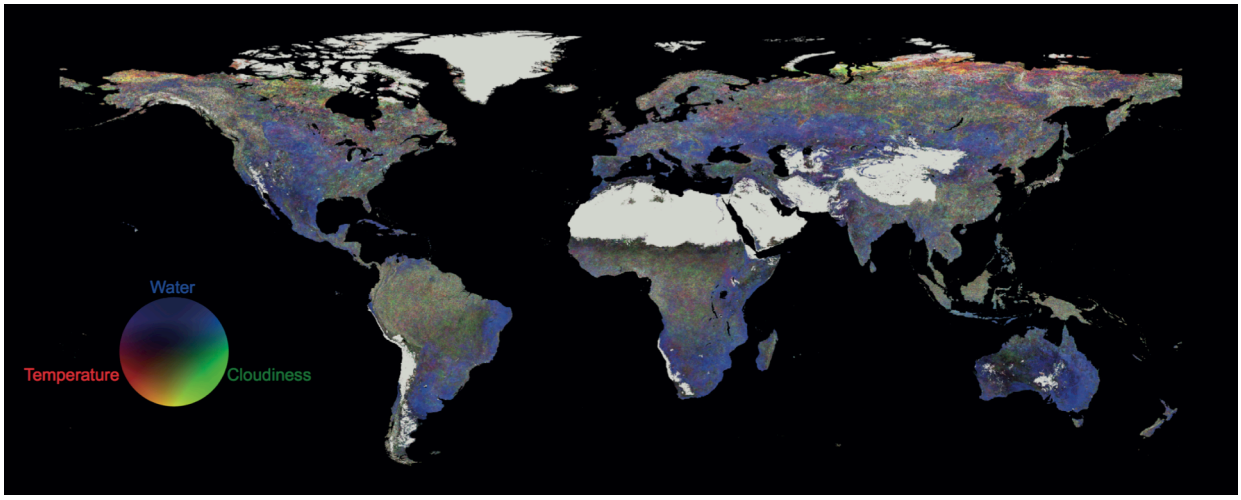


**Extended Data Figure 2 RGB composite of climate weights.** RGB composite global map of the mean climate coefficient weights from monthly multiple regressions between vegetation productivity (defined as EVI), vegetation productivity at $t-1$ and three climate variables (temperature, red; water availability, blue; and cloudiness, green). Areas with dominant barren land (mean EVI < 0.1 for all months) and permanent ice are shown grey. Pixel resolution, 5 km; period, 2000–2013.

Publisher: NPG; Journal: Nature: Nature; Article Type: Biology letter
DOI: 10.1038/nature16986

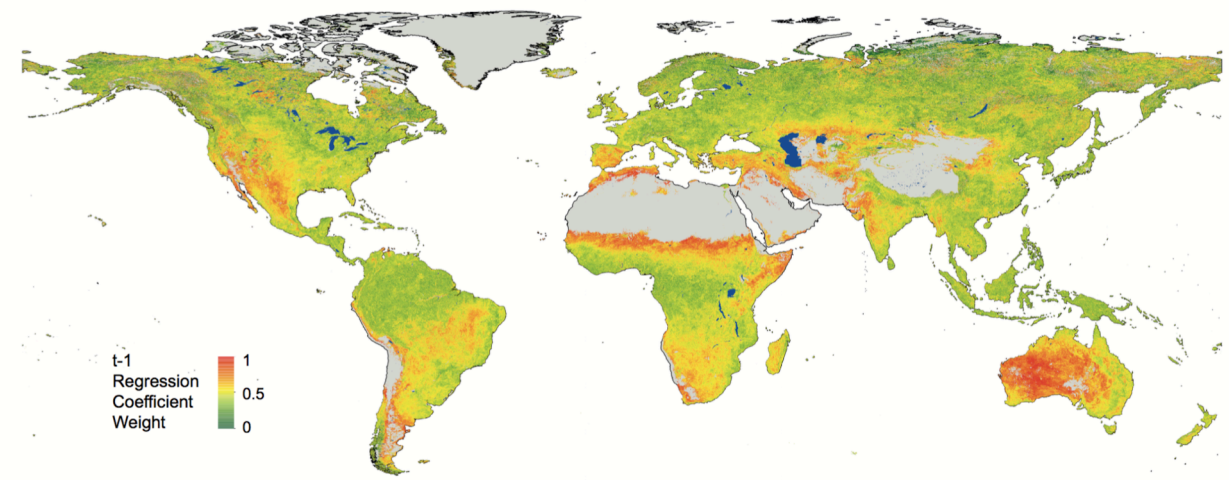


**Extended Data Figure 3 Global map of the *t*−1 coefficient.** Global map of *t*−1 (AR1) coefficient weight from a monthly multiple regressions between vegetation productivity (defined as EVI), vegetation productivity at *t*−1 and the three climate variables. Areas with dominant barren land (mean EVI <0.1 for all months) and permanent ice are shown grey. Wetland areas, as identified by the Global Lakes and Wetlands Database[30], are mapped in blue. Pixel resolution, 5 km; period, 2000–2013. Continental outlines were modified from a shapefile using ArcGIS 10.2 software (http://www.arcgis.com/home/item.html?id=a3cb207855b348a297ab85261743351d). ArcGIS and ArcMap are the intellectual property of Esri and are used herein under license.

Publisher: NPG; Journal: Nature: Nature; Article Type: Biology letter
DOI: 10.1038/nature16986

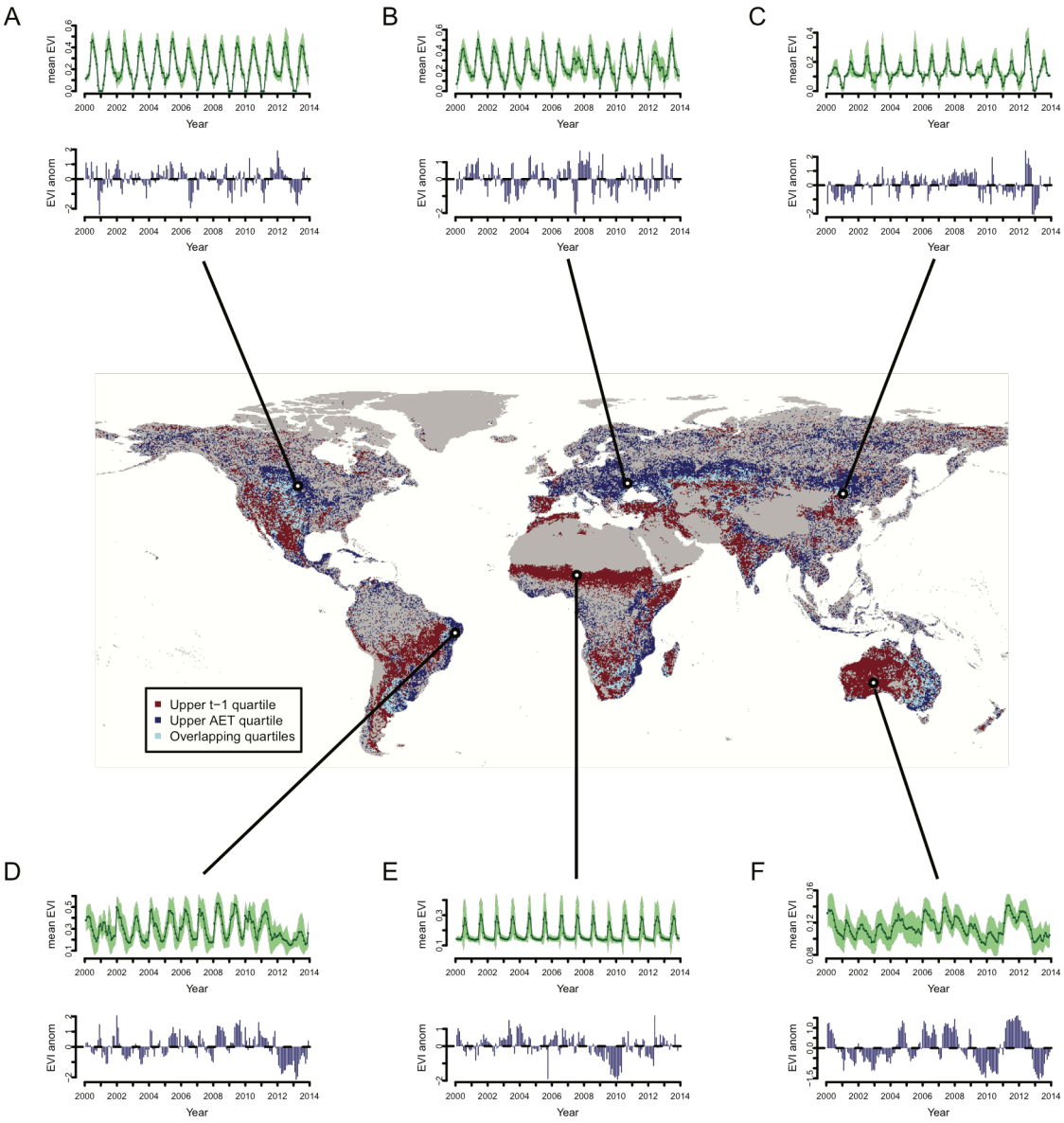


**Extended Data Figure 4 EVI variability in areas of low total annual precipitation.** Time series plots of the mean EVI (green) and mean EVI monthly anomalies (blue) for six different dryland/water-limited regions across the world. Time series are calculated by finding the mean monthly value for all 5-km pixels with a 1° grid cell (total pixels = 400). The light green shading in the mean EVI plots represents the upper and lower two standard deviations. A. North American temperate grassland (pixel centre 99.5° W, 47.5° N). B. Eurasian temperate grassland (30.5° E, 48.5° N). C. Eurasian temperate grassland (115.5 °E, 44.5 °N). D. Caatinga forests, woodlands and scrub (37.5° W, 8.5° S). E. Sahel subtropical savanna and shrubland (10.5° E, 13.5° N). F. Australian desert (127.5° E, 27.5° N). The map in the main panel insert represents areas with $t-1$ and water limitation linear regression coefficients within the upper quartile (see Methods). Red, $t-1$; dark blue, water limitation; light blue, both).

Publisher: NPG; Journal: Nature: Nature; Article Type: Biology letter
DOI: 10.1038/nature16986

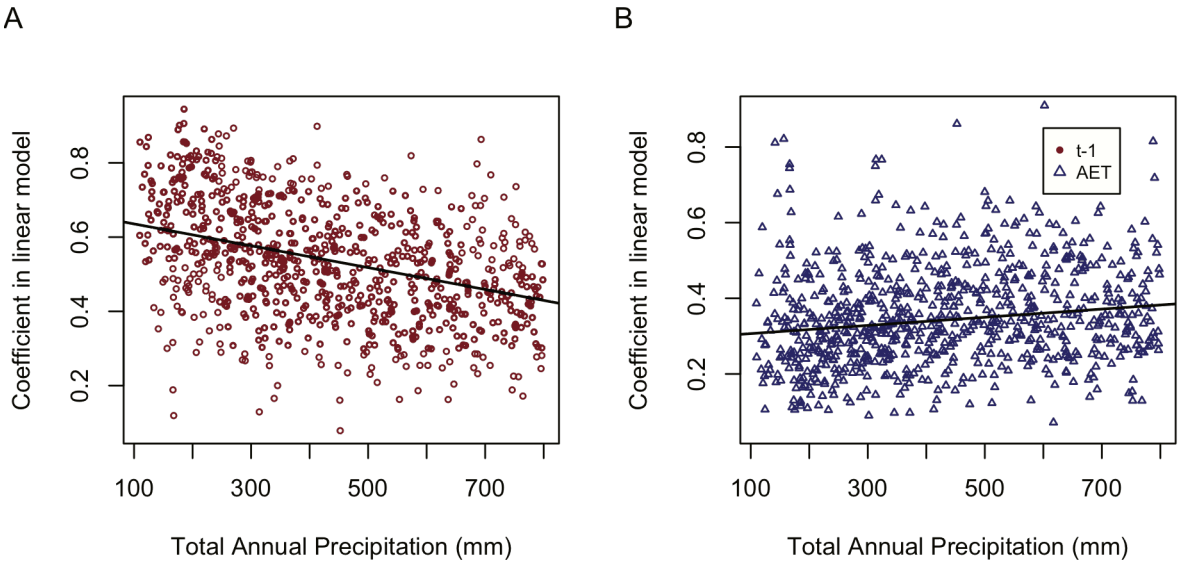


**Extended Data Figure 5 *t*−1 and water limitation against total annual precipitation.** Plots of the *t*−1 (A) and water limitation coefficients (B) from the AR1 linear regression model (see Methods) plotted against total annual precipitation (mm) calculated as the sum of the WorldClim monthly precipitation data[40]. A random subsample of 1,000 points were taken from dryland areas, defined here as having total annual precipitation between 100 – 800 mm, and between 50° N and 50° S. After removing no-data values from the random subset (that is, unresponsive pixels from the VSI calculation), the total number of samples was 795. A linear model was fit to both data sets independently using generalized least squares in the 'nlme'[36] package in R[34]. An exponential spatial error term using geographic distance was used to account for spatial autocorrelation in the residuals in the model[41]. There was a negative significant effect on the size of the *t*−1 coefficient with increasing total annual precipitation (−0.0003 ± 0.00003, significant at $P < 0.01$), with a smaller, positive effect of total annual precipitation on water availability (0.0001 ± 0.00003, significant at $P < 0.01$).

Publisher: NPG; Journal: Nature: Nature; Article Type: Biology letter
DOI: 10.1038/nature16986

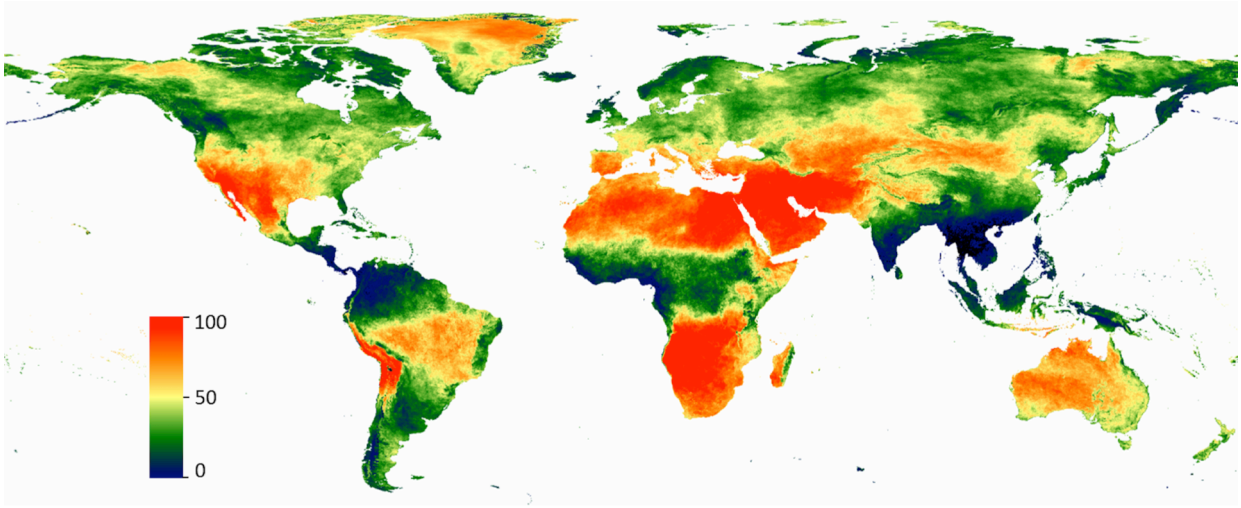


**Extended Data Figure 6 Cloudiness index.** Example output of the cloudiness index derived from the MOD35_L2 Cloud Mask product for June 2005. High values indicate more cloud-free days. Note the large number of cloud-free days in dryland regions, and the large number of cloudy days in southeast Asia as a result of the seasonal monsoon. Pixel resolution, 5 km.

Publisher: NPG; Journal: Nature: Nature; Article Type: Biology letter
DOI: 10.1038/nature16986

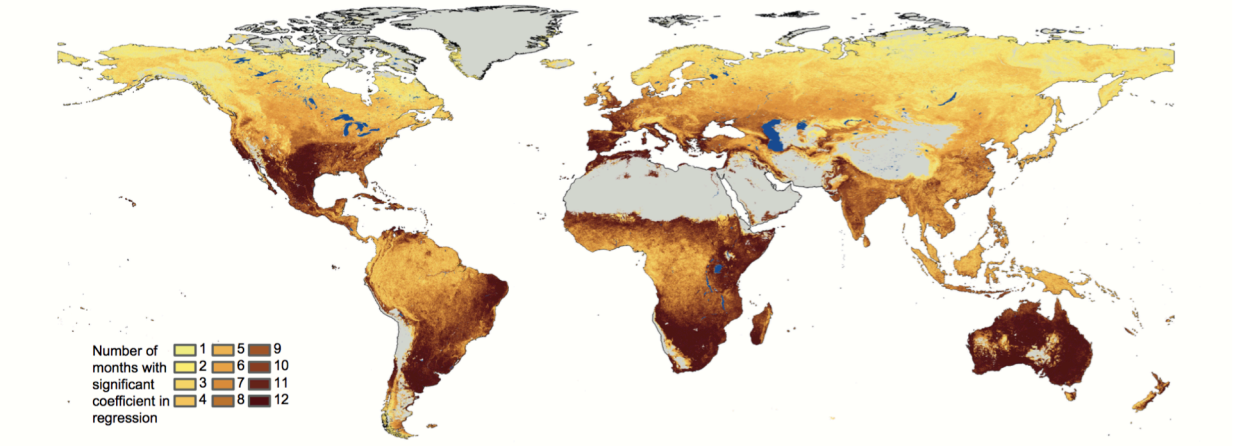


**Extended Data Figure 7 Number of months with a significant ($P < 0.1$) coefficient in the principal components regression.** Number of months with a significant ($P < 0.1$) coefficient in the principal components regression between vegetation productivity (EVI), and climate (temperature, water availability, and cloud cover), and a $t-1$ vegetation variable. Areas with dominant barren land (mean EVI < 0.1 for all months) and permanent ice are shown grey. Wetland areas, as identified by the Global Lakes and Wetlands Database[30], are mapped in blue. Pixel resolution, 5 km; period, 2000–2013. Continental outlines were modified from a shapefile using ArcGIS 10.2 software (http://www.arcgis.com/home/item.html?id=a3cb207855b348a297ab85261743351d). ArcGIS and ArcMap are the intellectual property of Esri and are used herein under license.

Publisher: NPG; Journal: Nature: Nature; Article Type: Biology letter
DOI: 10.1038/nature16986

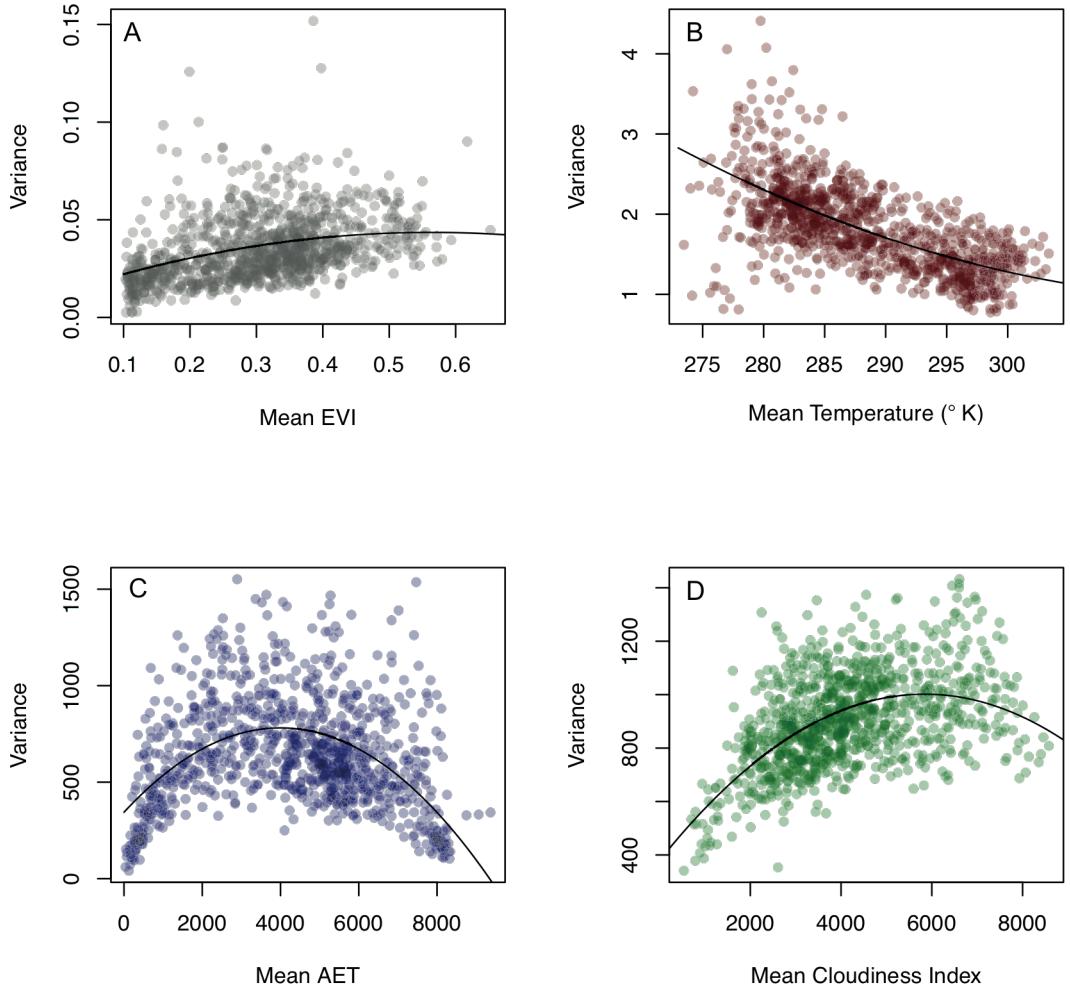


**Extended Data Figure 8 Mean–variance relationships. a–d**, Plots of the mean–variance relationships for EVI (**a**) and the three climate variables derived from MODIS data (ground temperature (**b**), water availability (**c**) and cloud cover (**d**)). Owing to the large number of pixels (7,200 × 3,000), these plots are made using 1,000 randomly sampled points from across the Earth surface for clarity.

Publisher: NPG; Journal: Nature: Nature; Article Type: Biology letter
DOI: 10.1038/nature16986

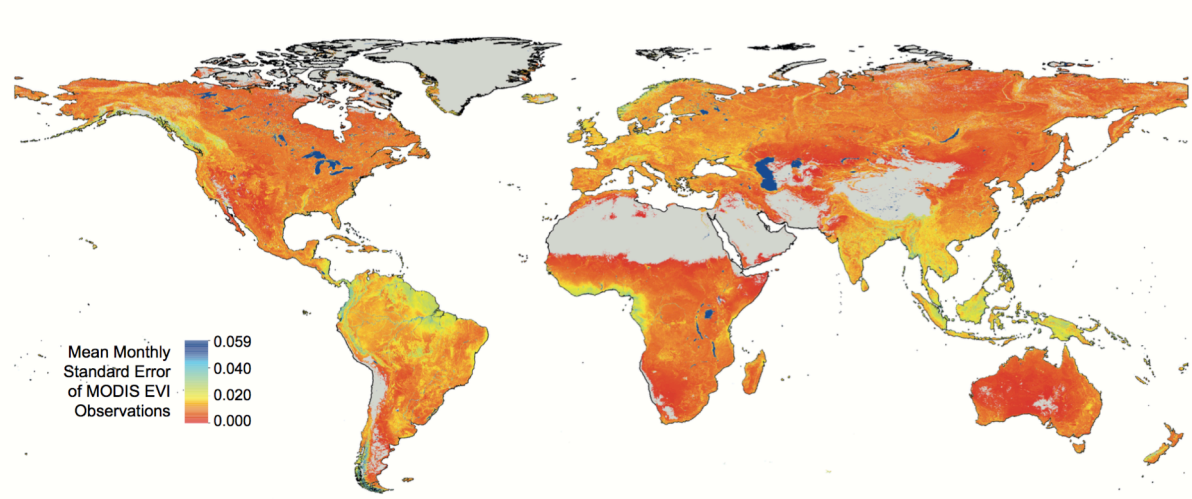


**Extended Data Figure 9 Mean standard error of the MODIS EVI observations.** Mean standard error of the MODIS EVI observations, calculated on a monthly basis over the period 2000–2013 as the standard deviation of all EVI observations per 5 km pixel divided by the square root of the number of observations. Areas with dominant barren land (mean EVI < 0.1 for all months) and permanent ice are shown grey. Wetland areas, as identified by the Global Lakes and Wetlands Database[30], are mapped in blue. Continental outlines were modified from a shapefile using ArcGIS 10.2 software (http://www.arcgis.com/home/item.html?id=a3cb207855b348a297ab85261743351d). ArcGIS and ArcMap are the intellectual property of Esri and are used herein under license.

Publisher: NPG; Journal: Nature: Nature; Article Type: Biology letter
DOI: 10.1038/nature16986

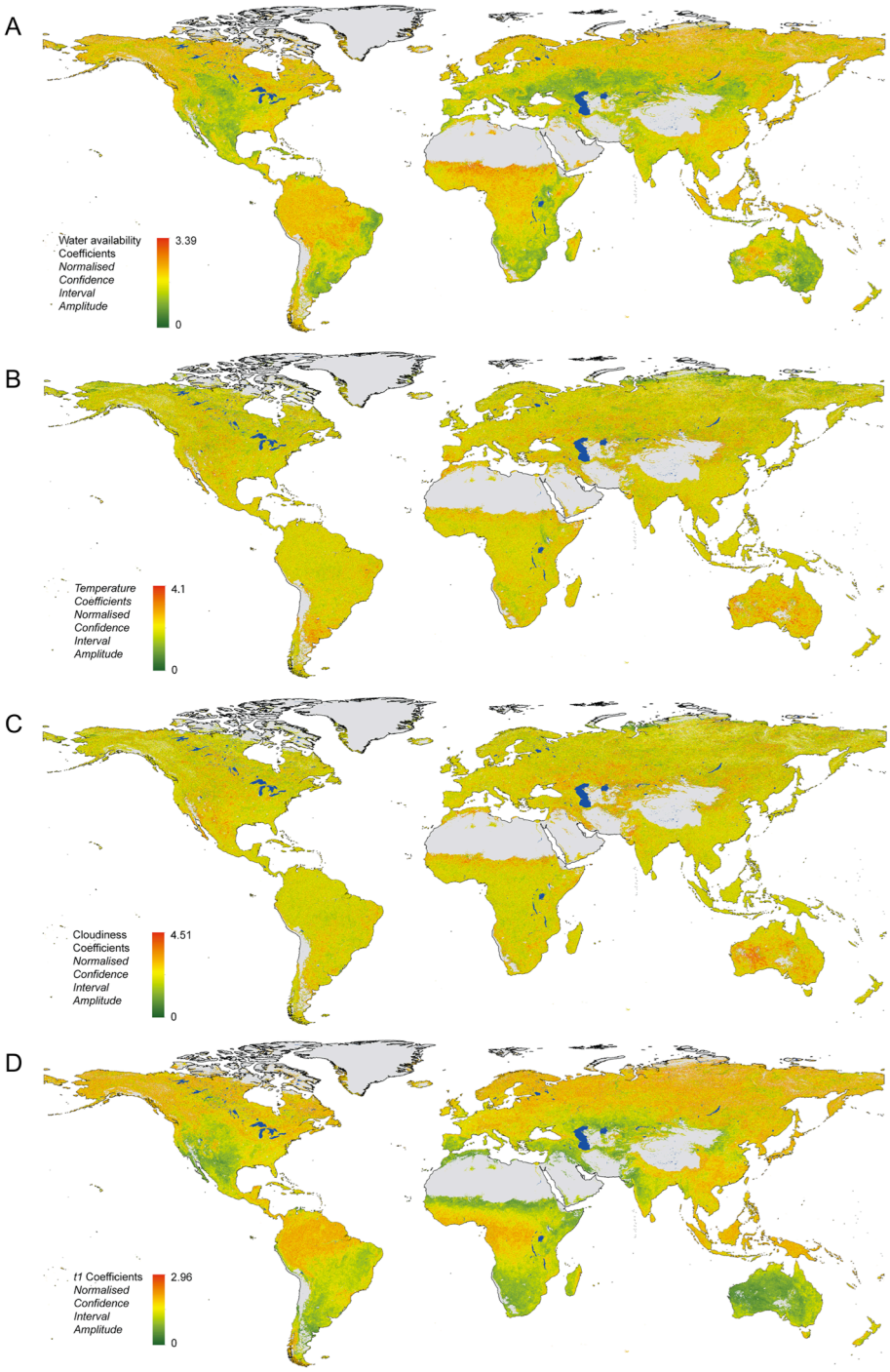


**Extended Data Figure 10 Normalized confidence interval amplitudes.** Normalized confidence interval amplitudes (NCIA) for the regression coefficients in the EVI versus external forcings (temperature, AET/PET, cloudiness) and memory effects (EVI $t-1$) regression. Larger NCIA values correspond to larger uncertainty in the coefficient estimates. Amplitudes were normalized by the mean coefficient value in each 5 km pixel (that is, a value of 2 corresponds to a total uncertainty twice as big

Publisher: NPG; Journal: Nature: Nature; Article Type: Biology letter
DOI: 10.1038/nature16986

as the coefficient value). Only significant coefficients in the original PCA regression were accounted for, and hence no coefficient crosses zero in any pixel. Areas with dominant barren land (mean EVI < 0.1 for all months) and permanent ice are shown grey. Wetland areas, as identified by the Global Lakes and Wetlands Database[30], are mapped in blue. **a**, Water availability; **b**, temperature; **c**, cloudiness; **d**, EVI $t-1$. Continental outlines were modified from a shapefile using ArcGIS 10.2 software (http://www.arcgis.com/home/item.html?id=a3cb207855b348a297ab85261743351d). ArcGIS and ArcMap are the intellectual property of Esri and are used herein under license.